

OGLE-2017-BLG-1522: A giant planet around a brown dwarf located in the Galactic bulge

Y. K. Jung^{1,10}, A. Udalski^{2,11}, A. Gould^{1,3,4,10}, Y.-H. Ryu^{1,10}, J. C. Yee^{5,10}

and

C. Han⁶, M. D. Albrow⁷, C.-U. Lee^{1,8}, S.-L. Kim^{1,8}, K.-H. Hwang¹, S.-J. Chung^{1,8},
I.-G. Shin⁵, W. Zhu³, S.-M. Cha^{1,9}, D.-J. Kim¹, Y. Lee^{1,9}, B.-G. Park^{1,8}, D.-J. Lee¹,
H.-W. Kim¹, R. W. Pogge⁴

(The KMTNet Collaboration)

M. K. Szymański², P. Mróz², R. Poleski^{2,3}, J. Skowron², P. Pietrukowicz²,
I. Soszyński², S. Kozłowski², K. Ulaczyk², M. Pawlak², K. Rybicki²

(The OGLE Collaboration)

¹*Korea Astronomy and Space Science Institute, Daejeon 34055, Republic of Korea*

²*Warsaw University Observatory, Al. Ujazdowskie 4, 00-478 Warszawa, Poland*

³*Department of Astronomy, Ohio State University, 140 W. 18th Ave., Columbus, OH
43210, USA*

⁴*Max-Planck-Institute for Astronomy, Königstuhl 17, 69117 Heidelberg, Germany*

⁵*Harvard-Smithsonian Center for Astrophysics, 60 Garden St., Cambridge, MA 02138,
USA*

⁶*Department of Physics, Chungbuk National University, Cheongju 28644, Republic of Korea*

⁷*University of Canterbury, Department of Physics and Astronomy, Private Bag 4800,
Christchurch 8020, New Zealand*

⁸*Korea University of Science and Technology, 217 Gajeong-ro, Yuseong-gu, Daejeon 34113,
Korea*

⁹*School of Space Research, Kyung Hee University, Yongin 17104, Republic of Korea*

ABSTRACT

¹⁰The KMTNet Collaboration.

¹¹The OGLE Collaboration.

We report the discovery of a giant planet in the OGLE-2017-BLG-1522 microlensing event. The planetary perturbations were clearly identified by high-cadence survey experiments despite the relatively short event timescale of $t_E \sim 7.5$ days. The Einstein radius is unusually small, $\theta_E = 0.065$ mas, implying that the lens system either has very low mass or lies much closer to the microlensed source than the Sun, or both. A Bayesian analysis yields component masses $(M_{\text{host}}, M_{\text{planet}}) = (46_{-25}^{+79}, 0.75_{-0.40}^{+1.26}) M_J$ and source-lens distance $D_{\text{LS}} = 0.99_{-0.54}^{+0.91}$ kpc, implying that this is a brown-dwarf/Jupiter system that probably lies in the Galactic bulge, a location that is also consistent with the relatively low lens-source relative proper motion $\mu = 3.2 \pm 0.5$ mas yr $^{-1}$. The projected companion-host separation is $0.59_{-0.11}^{+0.12}$ AU, indicating that the planet is placed beyond the snow line of the host, i.e., $a_{sl} \sim 0.12$ AU. Planet formation scenarios combined with the small companion-host mass ratio $q \sim 0.016$ and separation suggest that the companion could be the first discovery of a giant planet that formed in a protoplanetary disk around a brown dwarf host.

Subject headings: binaries: general – gravitational lensing: micro – brown dwarf – planetary systems

1. Introduction

Two decades after the first discoveries by Wolszczan & Frail (1992) and Mayor & Queloz (1995), about 4,000 extrasolar planets have been discovered¹. Most of these planets were detected by using the radial-velocity (e.g., Pepe et al. 2011) or transit (e.g., Tenenbaum et al. 2014) methods. Planets by these methods are detected indirectly from the observations of their host stars, and the hosts of the planets are overwhelmingly nearby Sun-like stars, with a mean and standard deviation of logarithmic mass of $\langle M_{\text{host,RV,trans}}/M_{\odot} \rangle = -0.027 \pm 0.148$.

On the other hand, the most common population of stars in the Milky Way Galaxy is low-mass M dwarfs, which are difficult to observe using the radial-velocity or transit methods². Our galaxy could also be teeming with brown dwarfs which cannot sustain hydrogen fusion and thus are very faint. It has been known that these very low-mass (VLM) objects can have circumstellar disks, which are believed to be formed by the process of grain growth,

¹NASA Exoplanet Archive, <http://exoplanetarchive.ipac.caltech.edu>

²The upcoming space missions such as the *Transiting Exoplanet Survey Satellite* (TESS: Ricker et al. 2014) will find transiting planets around M dwarf stars.

through dust settling, followed by crystallization (Apai et al. 2005; Riaz et al. 2012). If these disks can provide enough materials, then, planets can be formed in the disks of such low luminosity objects (Luhman 2012).

Studying planets around VLM objects are important not only because these objects are common but also because it can help us to better understand the planet formation mechanism. For example, the core accretion theory predicts that giant planets are difficult to be formed in the disks of low-mass stars (Ida & Lin 2004; Laughlin et al. 2004; Kennedy et al. 2006), hence the formation rate of giant planets in VLM objects should be low. By contrast, according to the disk instability mechanism (Boss 2006), giant planets can form in abundance and thus the giant-planet formation rate would be high. Therefore, determination of the planet formation rate based on a large unbiased sample of VLM objects can provide us with an important constraint on the planet formation mechanism.

Despite their usefulness, few planets orbiting VLM objects are known to date due to the observational difficulty caused by the faintness of planet hosts. Although some planetary systems were discovered by the direct imaging method (Chauvin et al. 2004; Todorov et al. 2010; Gauza et al. 2015; Stone et al. 2016), the sample is greatly biased toward planets with very wide separations ($\gg 1$ AU) from their hosts. Furthermore, it is difficult to spectroscopically determine the masses of the planets due to the faintness of the host combined with the extremely long orbital periods (Joergens & Muller 2007).

Microlensing can provide a complementary channel to detect and characterize planets around VLM objects. Since lensing effects occur solely by the gravity of a lensing object, the microlensing method is suitable to detect planets around faint or even dark VLM objects, implying no bias by the brightness of the planet hosts. Furthermore, the method is sensitive to planets in a wide separation range of $\sim 0.2 - 10$ AU, which cover the region of giant planet formation. The method already proved its usefulness by detecting planets around very low-mass host stars or brown dwarfs (e.g., Street et al. 2013; Furusawa et al. 2013; Han et al. 2013; Skowron et al. 2015; Shvartzvald et al. 2017; Nagakane et al. 2017).

In this paper, we report the discovery of a planet orbiting a brown dwarf from the analysis of the OGLE-2017-BLG-1522 microlensing event. Although the event timescale is relatively short, the anomaly is clearly captured from continuous observations of the Korea Microlensing Telescope Network (KMTNet: Kim et al. 2016) survey.

2. Observation

The OGLE-2017-BLG-1522 event occurred at $(\alpha, \delta)_{J2000} = (18^{\text{h}}01^{\text{m}}16^{\text{s}}.65, -28^{\circ}27'43''.1)$ $[(l, b) = (2.151^{\circ}, -2.179^{\circ})]$. It was discovered on 7 August 2017 by the Optical Gravitational Lensing Experiment (OGLE: Udalski et al. 2015) using the 1.3m Warsaw telescope at the Las Campanas Observatory in Chile, and announced from the Early Warning System (EWS: Udalski 2003)

The lensed star was also monitored by KMTNet. The KMTNet observations were carried out using three 1.6m telescopes located at the Cerro Tololo Inter-American Observatory in Chile (KMTC), South African Astronomical Observatory in South Africa (KMST), and Siding Spring Observatory in Australia (KMTA). The event lies in one of the pairs of its two offset fields (BLG03 and BLG43) with combined 4 hr^{-1} observation cadence. From this feature and with telescopes that are globally distributed, the KMTNet survey continuously and densely covered the event.

Data reductions were processed using pipelines of the individual groups (Udalski 2003; Albrow et al. 2009), which are based on the difference image analysis (DIA: Alard & Lupton 1998). For the usage of the data sets obtained from different observatories and reduced from different pipelines, we renormalized the errors of each data set. Following the procedure described in Yee et al. (2012), we adjusted the errors as

$$\sigma' = \sqrt{\sigma_{\text{min}}^2 + (k\sigma_0)^2}. \quad (1)$$

where σ_0 is the error determined from the pipeline and σ_{min} and k are the adjustment parameters. We note that the errors of OGLE data set were adjusted using the prescription discussed in Skowron et al. (2016). In Table 1, we present the correction parameters of individual data sets with the observed passbands and the number of data.

3. Analysis

As presented in Figure 1, the OGLE-2017-BLG-1522 light curve shows deviations from a standard single-mass lensing curve (Paczynski 1986). The deviations are composed of two major perturbations, one strong perturbation at $\text{HJD}' (= \text{HJD} - 2,450,000 \text{ days}) \sim 7971.4$ and the other weak short-term perturbation in the region between $7974 < \text{HJD}' < 7975$. The latter anomaly consists of a trough centered at $\text{HJD}' \sim 7974.6$ surrounded by bumps at both sides. Such a short-term anomaly is a characteristic feature that occurs when the source star crosses the small caustic induced by a low-mass companion to the primary lens. Therefore, we examine the event with the binary-lens interpretation.

To find the lensing parameters that describe the light curve, we adopt the parametrization and follow the procedure presented in Jung et al. (2015). We first carry out a preliminary grid search by setting s , q , and α as independent variables. Here s and q are, respectively, the projected separation (normalized to the angular Einstein radius, θ_E) and the mass ratio of the binary lens, and α is the trajectory angle. The grid space (s, q, α) is divided into $(100, 100, 21)$ grids and the ranges of individual variables are $-1.0 < \log s < 1.0$, $-4.0 < \log q < 0.0$, and $0 < \alpha < 2\pi$, respectively. We note that (s, q) are fixed, while α is allowed to vary at each grid point. From this search, we identify only one local minimum. It can be seen in Figure 2, where we show the derived $\Delta\chi^2$ surface in the (s, q) space. We then investigate the local solutions and find the global minimum by optimizing all parameters including grid variables with the Markov Chain Monte Carlo (MCMC) method.

In Table 2, we list the best-fit solution determined from our modeling. The model curve of the solution is presented in Figure 1. Also shown in Figure 3 is the corresponding lensing geometry. We find that the companion-host separation is $s = 1.21$ and the companion-host mass ratio is $q \sim 0.016$, implying that the companion would be in the planetary or substellar regime. In this case, the binary lens induces a single 6-sided resonant caustic near the host star (e.g., Dominik 1999). Although this caustic is resonant, it is very close to separating into a 4-sided “central caustic” (left) and a 4-sided “planetary caustic” (right), which it would do if s were only slightly larger than its actual value of $s = 1.21$. Specifically the transition would occur at (Erdl & Schneider 1993)

$$s_{\text{transition}} = \sqrt{\frac{(1 + q^{1/3})^3}{1 + q}} \rightarrow 1.39. \quad (2)$$

Hence, the cusps associated with the central-caustic wing of resonant caustic are strong, while those associated with the planetary-caustic wing are weak. The two major perturbations were generated by the source transit through the caustic. The first perturbation occurred when the source passed close to one of the central-caustic-wing cusps, while the other perturbation occurred when the source transited the caustic near one of the planetary-caustic-wing cusps.

We clearly detect finite-source effects from which the normalized source radius ρ_* and the angular Einstein radius θ_E is determined by

$$\theta_E = \frac{\theta_*}{\rho_*}. \quad (3)$$

Here the angular size of the source θ_* is estimated from the calibrated brightness $I_{0,S}$ and color $(V - I)_{0,S}$ of the source. To find $(V - I, I)_{0,S}$, we follow the procedure of Yoo et al. (2004). First, we build the instrumental color-magnitude diagram (CMD) using the KMTC Dophot reductions (Figure 4). Next, we estimate $(V - I, I)_{0,S}$ with the equation

$$(V - I, I)_{0,S} = (V - I, I)_S - (V - I, I)_{GC} + (V - I, I)_{0,GC}, \quad (4)$$

where $(V - I, I)_S$ and $(V - I, I)_{GC}$ are, respectively, the positions of the source and the giant clump (GC) centroid in the instrumental CMD, and $(V - I, I)_{0,GC} = (1.06, 14.34)$ is the calibrated position of the GC (Bensby et al. 2013; Nataf et al. 2013). From this, we find $(V - I, I)_{0,S} = (1.15 \pm 0.07, 20.61 \pm 0.09)$, indicating that the source is a K-type main-sequence star.

Once the source type is known, we determine θ_* using the *VIK* color-color relation (Bessell & Brett 1988) and the color-surface brightness relation (Kervella et al. 2004). The estimated angular size of the source is

$$\theta_* = 0.390 \pm 0.032 \text{ } \mu\text{as}, \quad (5)$$

which corresponds to the angular Einstein radius

$$\theta_E = 0.065 \pm 0.009 \text{ mas}. \quad (6)$$

With the measured Einstein timescale t_E , the geocentric proper motion of the source relative to the lens is then

$$\mu = \frac{\theta_E}{t_E} = 3.16 \pm 0.46 \text{ mas yr}^{-1}. \quad (7)$$

We note that the error in θ_* is derived from the uncertainty of the source brightness (4%) and the color-surface brightness conversion (7%). The errors of θ_E and μ are then estimated based on σ_{θ_*} and σ_{ρ_*} (see Table 2).

The Einstein radius is related to the total mass of the lens, M_{tot} , and the distance to the lens, D_L , by

$$\theta_E = \sqrt{\kappa M_{\text{tot}} \pi_{\text{rel}}} \sim 0.7 \text{ mas} \left(\frac{M_{\text{tot}}}{0.7 M_\odot} \right)^{1/2} \left(\frac{8 \text{ kpc}}{D_S} \right)^{1/2} \left(\frac{1-x}{x} \right)^{1/2}, \quad (8)$$

where $\kappa = 4G/(c^2 \text{AU})$, $\pi_{\text{rel}} = \text{AU}(D_L^{-1} - D_S^{-1})$, D_S is the distance to the source, and $x = D_L/D_S$. Then, the derived θ_E is significantly smaller than $\theta_E \sim 0.7$ mas of an event caused by a stellar object with $M_{\text{tot}} \sim 0.7 M_\odot$ and $x \sim 0.5$. This suggests that the event was generated by a VLM binary and/or a lens system located in the Galactic bulge very close to the source, i.e., $x \sim 1.0$.

4. Physical Parameters

The direct measurement of M_{tot} and D_L of the lens system requires the simultaneous detection of θ_E and the microlens parallax π_E , i.e.,

$$M_{\text{tot}} = \frac{\theta_E}{\kappa \pi_E}; \quad D_L = \frac{\text{AU}}{\pi_E \theta_E + \pi_S}, \quad (9)$$

where $\pi_S = \text{AU}/D_S$ is the source parallax (Gould 1992, 2004). For OGLE-2017-BLG-1522, the angular Einstein radius is measured, but the microlens parallax cannot be measured, and thus the physical properties cannot be directly determined. Therefore, we investigate the probability distributions of physical parameters from the measured θ_E and t_E . For this, we perform a Bayesian analysis using a Galactic model based on the velocity distribution (VD), mass function (MF), and matter density profile (DP) of the Milky Way Galaxy.

In order to construct the model, we define the Cartesian coordinates in the Galactic frame so that the center of the coordinates is the Galactic center and the x -axis and the z -axis point toward the Earth and the north Galactic pole, respectively. Then, the line of sight distance D of an object is related to the Galactic coordinates by

$$x = R_\odot - D\cos(l)\cos(b), \quad y = D\sin(l)\cos(b), \quad z = D\sin(b), \quad (10)$$

where $R_\odot = 8 \text{ kpc}$ is the adopted Galactocentric distance of the Sun (Reid 1993; Gillessen et al. 2013).

For the VD, we adopt the Han & Gould (1995) model of $f(v_y, v_z) = f(v_y)f(v_z)$ which follows a Gaussian form, i.e.,

$$f(v_y) = \frac{1}{\sqrt{2\pi\sigma_y^2}} \exp\left[-\frac{(v_y - \bar{v}_y)^2}{2\sigma_y^2}\right] \quad (11)$$

and a similar form for $f(v_z)$. Here \bar{v} and σ denote the mean and dispersion of the velocity component, respectively. Following Han & Gould (1995), we use $(\bar{v}_{z,\text{bulge}}, \bar{v}_{z,\text{disk}}) = (0, 0) \text{ km s}^{-1}$ and $(\sigma_{z,\text{bulge}}, \sigma_{z,\text{disk}}) = (100, 20) \text{ km s}^{-1}$ for the z -direction and $(\bar{v}_{y,\text{bulge}}, \bar{v}_{y,\text{disk}}) = (0, 220) \text{ km s}^{-1}$ and $(\sigma_{y,\text{bulge}}, \sigma_{y,\text{disk}}) = (100, 30) \text{ km s}^{-1}$ for the y -direction. For a given set of the projected velocity of the lens \mathbf{v}_L , the source \mathbf{v}_S , and the observer \mathbf{v}_o , the transverse velocity of the lens with respect to the source \mathbf{v} is then given by

$$\mathbf{v} = \mathbf{v}_L - \left[\mathbf{v}_S \frac{D_L}{D_S} + \mathbf{v}_o \frac{D_S - D_L}{D_S} \right]. \quad (12)$$

The projected velocity of the observer \mathbf{v}_o is estimated by converting the heliocentric Earth's velocity at the peak time of the event, $\mathbf{v}_E = (v_{E,E}, v_{E,N}) = (21.07, -1.75) \text{ km s}^{-1}$, to the Galactic frame. In this procedure, we also consider the peculiar and circular motion of the Sun with respect to a local standard of rest, i.e., $\mathbf{v}_\odot = \mathbf{v}_{\odot,\text{pec}} + \mathbf{v}_{\odot,\text{cir}} = (12, 7) + (220, 0) \text{ km s}^{-1}$.

For the MF, we separately consider the bulge and the disk lens populations. We model the bulge population by adopting the log-normal initial mass function (IMF: Chabrier 2003), while we model the disk population by adopting the log-normal present-day mass function

(PDMF: Chabrier 2003). In both functions, the lower mass limit is set to $0.01 M_{\odot}$. We note that we do not consider stellar remnants, since planets orbiting a star in the phase of asymptotic giant branch or planetary nebular would be hard to survive, and thus the probability to find planets orbiting a remnant would be extremely low (e.g., Kilic et al. 2009).

For the DP, we use a triaxial profile for the bulge and a double exponential profile for the disk. In the case of bulge profile, we adopt the refined Han & Gould (2003) model for which the profile follows the Dwek et al. (1995) model and the density is normalized by the star count results of Holtzman et al. (1998). The disk profile is modeled by the two (thin and thick disk) exponential disks of the form

$$\rho_{r,z} = \rho(R_{\odot}, 0)e^{R_{\odot}/h_R}\exp\left(-\frac{r}{h_R} - \frac{z + z_{\odot}}{h_Z}\right), \quad (13)$$

where $r = (x^2 + y^2)^{1/2}$, z_{\odot} is the offset of the Sun from the Galactic plane, and h_R and h_Z are the radial and vertical scale length, respectively. We adopt $z_{\odot} = 25$ pc, $(h_R, h_Z)_{\text{thin}} = (2600, 300)$ pc, $(h_R, h_Z)_{\text{thick}} = (3600, 900)$ pc, and the normalization factor $f = \rho_{\text{thick}}(R_{\odot}, 0)/\rho_{\text{thin}}(R_{\odot}, 0) = 0.12$ from Jurić et al. (2008), where they construct the profile using stellar objects detected by the Sloan Digital Sky Survey (SDSS: York et al. 2000). Finally, we normalize the number density to $\rho(R_{\odot}, 0) = 0.05 M_{\odot} \text{ pc}^{-3}$ by following the disk density of solar neighborhood estimated by Han & Gould (2003).

With the adopted models of VD, MF, and DP, we generate microlensing events from the Monte Carlo simulation and then investigate the probability distributions of the host mass M_1 and lens distance using the measured θ_E and t_E as a prior ³. In Figure 5, we show the posterior probabilities of M_1 (upper panel) and D_L (lower panel) derived from our Bayesian analysis. The median value of the mass and the distance with 68% (1σ) confidence intervals are

$$M_1 = 0.045_{-0.024}^{+0.076} M_{\odot}, \quad D_L = 7.49_{-0.88}^{+0.91} \text{ kpc}, \quad (14)$$

respectively. The estimated host star corresponds to a brown dwarf. The median value of the lens distance implies that both the lens and the source are likely to be located in the Galactic bulge. These consequently indicate that the extraordinarily small value of θ_E is due to the combination of the small lens mass and the lens location close to the source.

³We note that we apply the bulge model for the source by assuming that the source is in the bulge, while we separately apply the bulge and disk models for the lens. We then estimate the total probabilities by summing each set of the distribution.

From the measured q , the companion mass is determined by

$$M_2 = qM_1 = 0.75_{-0.40}^{+1.26} M_J, \quad (15)$$

which roughly corresponds to the Jupiter mass planet. The physical companion-host projected separation is

$$a_{\perp} = sD_L\theta_E = 0.59_{-0.11}^{+0.12} \text{ AU}. \quad (16)$$

By adopting that the snow line scales with the host mass (Kennedy & Kenyon 2008), we estimate the snow line of the lens system by $a_{sl} = 2.7 \text{ AU}(M/M_{\odot}) \sim 0.12 \text{ AU}$, indicating that the giant planet is placed beyond the snow line.

5. Discussion

We found a planetary candidate around a probable brown dwarf host located in the Galactic bulge. The probability that the host is a brown dwarf (i.e., $M_1 < 0.08 M_{\odot}$) is $\sim 76\%$ (see Figure 5). The light curve perturbations were clearly identified by the OGLE survey and continuously covered by the KMTNet observations despite the relatively short event timescale ($t_E \sim 7.5$ days), which enabled the unambiguous characterization of the lens system. This proves the capability of current microlensing experiments. In Figure 6, we compare the mass distribution of the lens to those of known exoplanets. From this, we find that this event could be the first binary that closes the gap between terrestrial and jovian mass companions in the brown-dwarf host region. We also find that MOA-2013-BLG-605 could have similar properties to our results (Sumi et al. 2016). However, it not only suffers from large uncertainties ($3 \sim 21 M_{\oplus}$ for the companion and $0.03 \sim 0.2 M_{\odot}$ for the host) due to the severe degeneracy in the parallax measurement but also favors the terrestrial planet interpretation. It is worth noting that the analysis of a large sample of short-timescale binary events found by Mróz et al. (2017) can bring additional information on the population of planetary-mass companions to brown dwarf hosts.

Up to now, several brown dwarfs hosting giant planet companions have been discovered. However, their large mass ratios ($q \gtrsim 0.1$) between the host and the companion would suggest that they are formed as binary systems either by the dynamical interaction in unstable molecular clouds (Bate 2009, 2012) or by the turbulent fragmentation of molecular cloud cores (Padoan & Nordlund 2004). This implies that the companions could be considered as substellar objects rather than planets (Chabrier et al. 2014). By contrast, the low mass ratio of this event ($q \sim 0.016$), combined with recent reports of the massive disks ($\gtrsim M_J$) around young brown dwarfs (Hervey et al. 2012; André et al. 2012; Palau et al. 2014), suggest that the planetary companion of the event may be formed by planet formation mechanisms.

Therefore, OGLE-2017-BLG-1522Lb could be the first giant planet orbiting around a brown-dwarf host having a planetary mass ratio.

It would therefore be of considerable interest to make a definitive determination of whether the host is a brown dwarf or a star. Considering that the measured relative source motion is $\mu \sim 3 \text{ mas yr}^{-1}$, the source will be separated from the lens about $\gtrsim 30 \text{ mas}$ at first light of the upcoming next generation ($D \sim 30\text{m}$ class) telescopes. Then, the source and the lens could be resolved with these telescopes because their resolution in H band will be $\theta = 14(D/30\text{m})^{-1} \text{ mas}$. Hence, at first light for any of these telescopes, the source and lens will be separated by well over 1 FWHM. If the host is a star rather than a brown dwarf, $M > 0.08 M_{\odot}$, then $M_{H,\text{host}} \lesssim 9$ and $\pi_{\text{rel}} < 6.4 \mu\text{as}$, i.e., $D_L \sim 8 \text{ kpc}$. The H band magnitude of the host is then $H_{\text{host}} \lesssim 23.5$ which should be easily visible in AO images. As a result, the nature of the host (star or brown dwarf) can be unambiguously resolved at that time.

This research has made use of the KMTNet system operated by the Korea Astronomy and Space Science Institute (KASI) and the data were obtained at three host sites of CTIO in Chile, SAAO in South Africa, and SSO in Australia. OGLE project has received funding from the National Science Centre, Poland, grant MAESTRO 2014/14/A/ST9/00121 to AU. C. Han was supported by grant 2017R1A4A1015178 of the National Research Foundation of Korea. Work by WZ, YKJ, and AG were supported by AST-1516842 from the US NSF. WZ, IGS, and AG were supported by JPL grant 1500811. AG is supported from KASI grant 2016-1-832-01.

REFERENCES

- Alard, C., & Lupton, Robert H. 1998, ApJ, 503, 325
- Albrow, M. D., Horne, K., Bramich, D. M., et al. 2009, MNRAS, 397, 2099
- André, P., Ward-Thompson, D., & Greaves, J. 2012, Sci, 337, 69
- Apai, D., Pascucci, I., Bouwman, J., et al. 2005, Sci, 310, 834
- Bate, M. R. 2009, MNRAS, 392, 590
- Bate, M. R. 2012, MNRAS, 419, 3115
- Bensby, T., Yee, J. C., Feltzing, S., et al. 2013, A&A, 549, 147
- Bessell, M. S., & Brett, J. M. 1988, PASP, 100, 1134

- Boss, A. P. 2006, *ApJ*, 643, 501
- Chabrier, G. 2003, *PASP*, 115, 763
- Chabrier, G., Johansen, A., Janson, M., & Rafikov, R. 2014, in *Protostars and Planets VI, Giant Planet and Brown Dwarf Formation*, ed. H. Beuther et al. (Tucson, AZ: Univ. Arizona Press), 619
- Chauvin, G., Lagrange, A. M., Dumas, C., et al. 2004, *A&A*, 425, L29
- Chen, J., & Kipping, D. 2017, *ApJ*, 834, 17
- Dominik, M. 1999, *A&A*, 349, 108
- Dwek, E., Arendt, R. G., Hauser, M. G., et al. 1995, *ApJ*, 445, 716
- Erdl, H., & Schneider, P. 1993, *A&A*, 268, 453
- Furusawa, K., Udalski, A., Sumi, T., et al. 2013, *ApJ*, 779, 91
- Gauza, B., Béjar, V. J. S., Prez-Garrido, A., et al. 2015, *ApJ*, 804, 96
- Gillessen, S., Eisenhauer, F., Fritz, T. K., et al. 2013, in *IAU Symp. 289, Advancing the Physics of Cosmic Distances*, ed. R. de Grijs (Cambridge: Cambridge Univ. Press), 29
- Gould, A. 1992, *ApJ*, 392, 442
- Gould, A. 2004, *ApJ*, 606, 319
- Han, C., & Gould, A. 1995, *ApJ*, 447, 53
- Han, C., & Gould, A. 2003, *ApJ*, 592, 172
- Han, C., Jung, Y. K., Udalski, A., et al. 2013, *ApJ*, 778, 38
- Harvey, P. M., Henning, Th., Liu, Y., et al. 2012, *ApJ*, 755, 67
- Holtzman, J. A., Watson, A. M., Baum, W. A., et al. 1998, *AJ*, 115, 1946
- Ida, S., & Lin, D. N. C. 2004, *ApJ*, 616, 567
- Joergens, V., & Muller, A. 2007, *ApJ*, 666, L113
- Jung, Y. K., Udalski, A., Sumi, T., et al. 2015, *ApJ*, 798, 123

- Jurić, M., Ivezić, Z., Brooks, A., et al. 2008, *ApJ*, 673, 864
- Kennedy, G. M., Kenyon, S. J., & Bromley, B. C. 2006, *ApJ*, 650, L139
- Kennedy, G. M., & Kenyon, S. J. 2008, *ApJ*, 673, 502
- Kervella P., Thévenin F., Di Folco E., Ségransan D., 2004, *A&A*, 426, 297
- Kilic, M., Gould, A., & Koester, D. 2009, *ApJ*, 705, 1219
- Kim, S.-L., Lee, C.-U., Park, B.-G., et al. 2016, *JKAS*, 49, 37
- Laughlin, G., Bodenheimer, P., & Adams, F. C. 2004, *ApJ*, 612, L73
- Luhman, K. L. 2012, *ARA&A*, 50, 65
- Mayor, M., & Queloz, D. 1995, *Nature*, 378, 355
- Mróz, P., Udalski, A., Skowron, J. et al. 2017 *Nature*, 548, 183
- Nagakane, M., Sumi, T., Koshimoto, N., et al. 2017, *AJ*, 154,35
- Nataf, D. M., Gould, A., Fouqué, P., et al. 2013, *ApJ*, 769, 88
- Paczynski, B. 1986, *ApJ*, 304, 1
- Padoan, P., & Nordlund, A. 2004, *ApJ*, 617, 559
- Palau, A., Zapata, L. A., Rodríguez, L. F., et al. 2014, *MNRAS*, 444, 833
- Pepe, F., Lovis, C., & Ségransan, D. 2011, *A&A*, 534, A58
- Reid, M. J. 1993, *ARA&A*, 31, 345
- Ricker, G. R., Winn, J. N., Vanderspek, R., et al. 2014, *JATIS*, 1, 014003
- Riaz, B., Lodieu, N., Goodwin, S., Stamatellos, D., & Thompson, M. 2012, *MNRAS*, 420, 2497
- Shvartzvald, Y., Yee, J. C., Calchi Novati, S., et al. 2017, *ApJ*, 840, L3
- Skowron, J., Shin, I.-G., Udalski, A., et al. 2015, *ApJ*, 804, 33
- Skowron, J., Udalski, A., Kozłowski, S., et al. 2016, *Acta Astron.*, 66, 1
- Stone, J. M., Skemer, A. J., Kratter, K. M., et al. 2016, *ApJ*, 818, L12

- Street, R. A., Choi, J.-Y., Tsapras, Y., et al. 2013, *ApJ*, 763, 67
- Tenenbaum, P., Jenkins, J. M., Seader, S., et al. 2014, *ApJS*, 211, 6
- Todorov, K., Luhman, K. L., & Mcleod, K. K. 2010, *ApJ*, 714, L84
- Spiegel, D. S., Burrows, A., & Milsom, J. A. 2011, *ApJ*, 727, 57
- Sumi, T., Udalski, A., Bennett, D. P., et al. 2016 *ApJ*, 825, 112
- Udalski, A. 2003, *Acta Astron.*, 53, 291
- Udalski, A., Szymański, M. K., & Szymański, G. 2015, *Acta Astron*, 65, 1
- Wolszczan, A., & Frail, D. A. 1992, *Nature*, 355, 145
- Yee, J. C., Shvartzvald, Y., Gal-Yam, A., et al. 2012, *ApJ*, 755, 102
- Yoo, J., DePoy, D. L., Gal-Yam, A., et al. 2004, *ApJ*, 603, 139
- York, D. G., Adelman, J., Anderson, J. E., et al. 2000, *AJ*, 120, 1579

Table 1. Error Correction Parameters

Observatory	Number	k	σ_{\min} (mag)
OGLE (I)	11365	1.672	0.002
KMTC BLG03 (I)	1336	1.153	0.000
KMTC BLG43 (I)	1639	1.438	0.000
KMTS BLG03 (I)	2323	1.268	0.000
KMTS BLG43 (I)	2173	1.389	0.000
KMTA BLG03 (I)	1787	1.679	0.000
KMTA BLG43 (I)	1818	1.506	0.000

Table 2. Lensing Parameters

Parameters	Values
χ^2/dof	21009.3/22434
t_0 (HJD')	7971.80 ± 0.01
u_0 (10^{-2})	5.39 ± 0.34
t_E (days)	7.53 ± 0.28
s	1.21 ± 0.01
q (10^{-2})	1.59 ± 0.16
α (rad)	6.22 ± 0.01
ρ_* (10^{-2})	0.60 ± 0.07
f_S	0.035 ± 0.002
f_B	2.221 ± 0.002

Note. — $\text{HJD}' = \text{HJD} - 2,450,000$ days

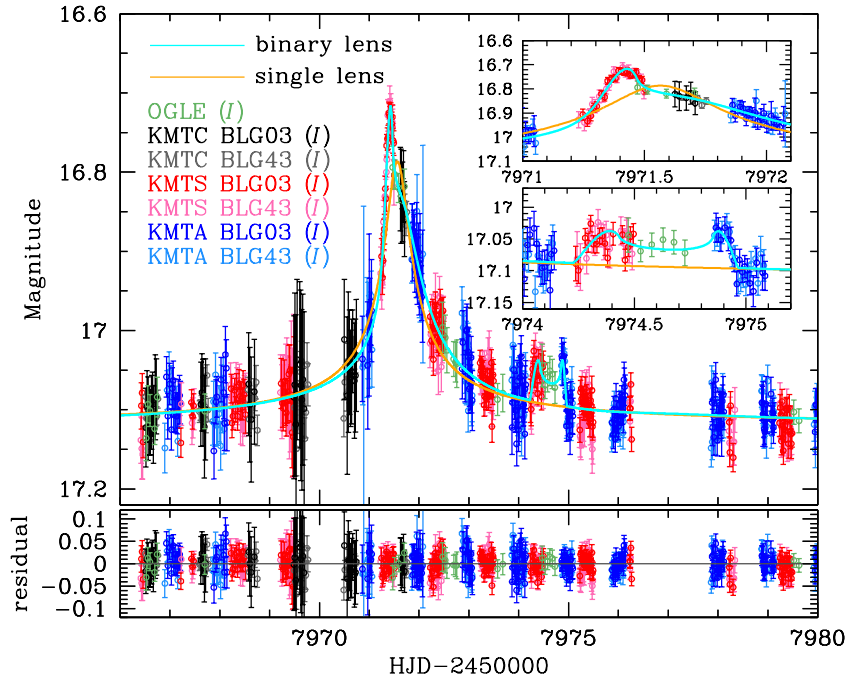


Fig. 1.— Light curve of OGLE-2017-BLG-1522. The upper and lower insets show the zoom of two major perturbations centered at $\text{HJD}' \sim 7971.4$ and 7974.6 , respectively. The cyan curve is the model curve based on the binary-lens interpretation, while the orange curve is based on the single-lens interpretation.

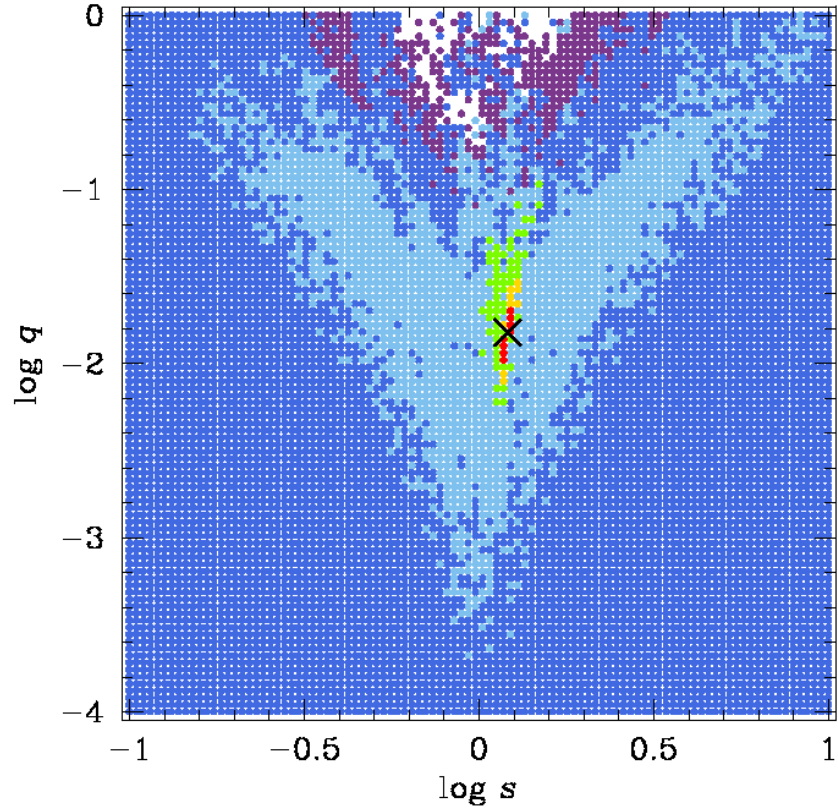


Fig. 2.— $\Delta\chi^2$ surface in (s, q) space obtained from the grid search. The space is color coded by $\Delta\chi^2 < 5^2$ (red), $< 10^2$ (yellow), $< 15^2$ (green), $< 20^2$ (light blue), $< 25^2$ (blue), and $< 30^2$ (purple) level, respectively. The cross mark is the location of the best-fit solution.

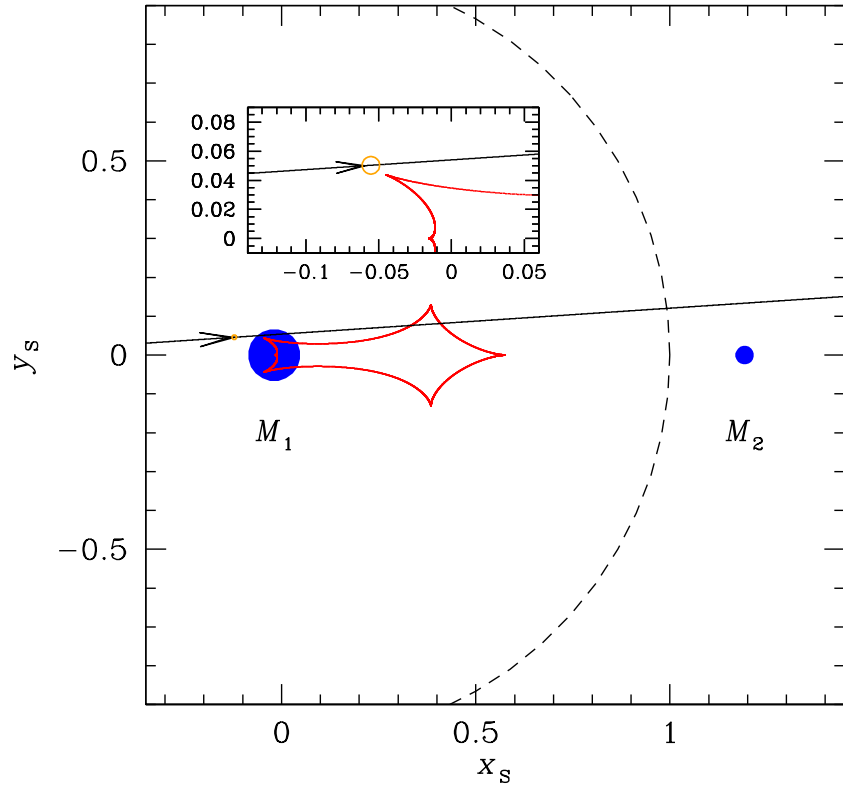


Fig. 3.— Geometry of the best-fit solution. The red closed curve is the caustic, the two blue dots (M_1 and M_2) are the positions of binary-lens components, and the orange circle is the size of the source. The dashed circle is the angular Einstein ring of the lens system and all lengths are scaled to its radius θ_E .

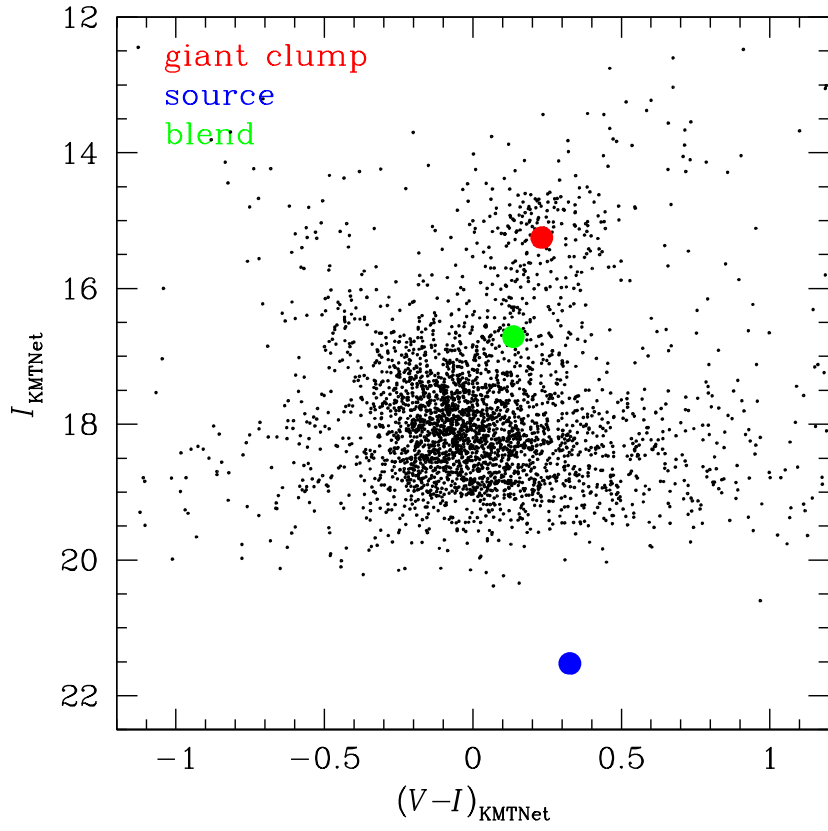


Fig. 4.— Position of the source star (blue dot) relative to the GC centroid (red dot) in the $(V - I, I)$ CMD of field stars around OGLE-2017-BLG-1522. The green dot is the position of blended light.

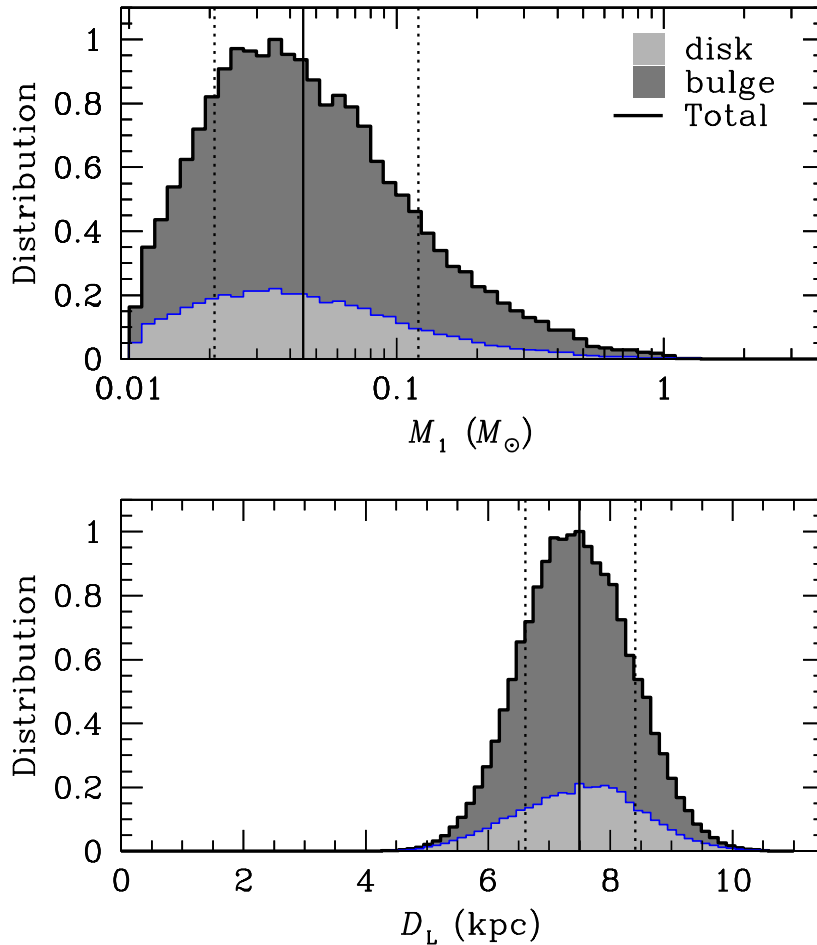


Fig. 5.— Probability distributions of the host mass (upper panel) and lens distance (lower panel) derived from the Bayesian analysis. The grey and darkgrey distributions are those derived from the disk and bulge Galactic models, respectively. In each panel, the solid line represents the median value and the two dotted lines represent the confidence intervals estimated based on the lower and upper boundaries encompassing the 68% (1σ) range of the distribution.

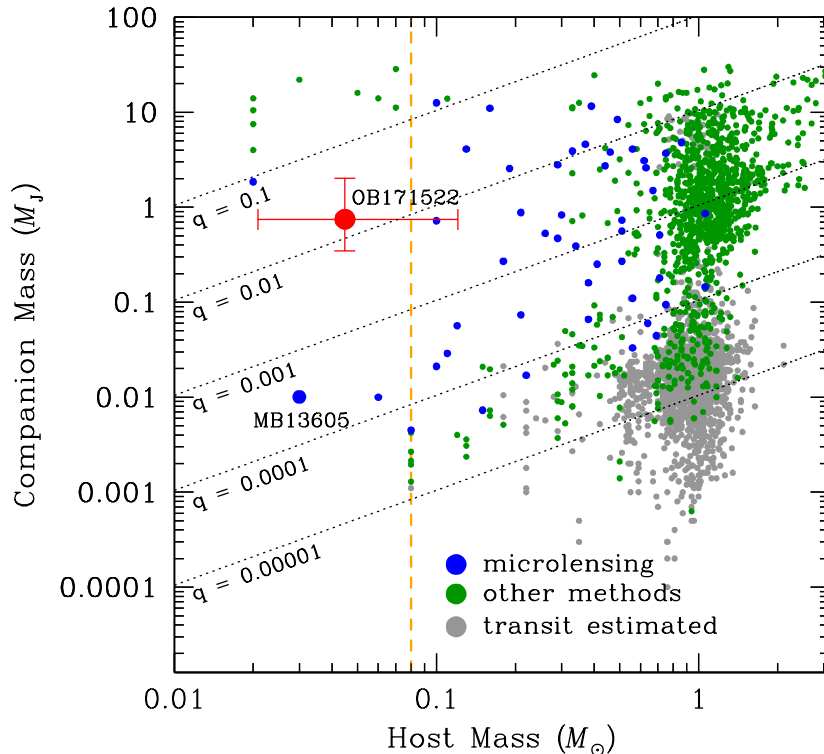


Fig. 6.— Mass distribution of known exoplanets. The red dot is OGLE-2017-BLG-1522. The planets discovered by microlensing method are marked by blue dots, while those found by other methods are marked by green dots. For transiting systems for which companion masses are not directly determined, we estimate the companion mass using the forecasting model of Chen & Kipping (2017) (grey dots). The yellow vertical dashed line represents the conventional star/brown-dwarf boundary. The values are acquired from <http://exoplanetarchive.ipac.caltech.edu>.